Journal of Engineering Mechanics and Machinery (2025)
Clausius Scientific Press, Canada

DOI: 10.23977/jemm.2025.100202
ISSN 2371-9133 Vol. 10 Num. 2

Mechanical Performance of Yurt Assemblies: A Finite Element Analysis Approach

Zhiru Wang

Beijing No.4 High School International Campus, No. 2J, West Huangchenggen North Street, Xicheng District, Beijing, 100034, China
huduchonglove@163.com

Keywords: Yurt; Finite Element Analysis; Structural Mechanics; Wind Load; Safety Factor

Abstract: This study presents a comprehensive finite element analysis (FEA) of the structural behavior of yurt assemblies subjected to extreme loading conditions, including a gravity load of 180 N and a wind load of 1984.5 N. The modeling process encompasses the geometric definition of nodes and elements, formulation of element stiffness matrices, coordinate transformations, global stiffness matrix assembly, imposition of loads and boundary conditions, and computation of nodal displacements and internal forces. The analysis reveals that the yurt structure exhibits stable mechanical performance under the specified loading conditions, with a maximum apex displacement of only 3.5 mm. Internal force distribution aligns with fundamental principles of structural mechanics: vertical support members sustain the highest compressive force (268.3 N), while bottom horizontal members primarily undergo tensile loading (142.1 N). The maximum compressive and tensile stresses are found to be 0.89 MPa and 0.47 MPa, respectively. When compared to the yield strength of steel (235 MPa), the corresponding safety factors are approximately 264 and 500, significantly surpassing standard design criteria. These findings underscore the structural efficiency and high safety factor of yurt configurations under combined loading scenarios.

1. Introduction

The yurt, also known as the Mongolian ger, is a traditional dwelling passed down through generations of nomadic peoples. Over centuries, it has evolved into a distinctive architectural form characterized by its portability, modularity, and exceptional adaptability to diverse environmental conditions. Beyond its functional role, the yurt embodies the ingenuity of ancestral engineering, serving as a material manifestation of nomadic culture and an enduring symbol of steppe civilization. In recent years, the resurgence of interest in sustainable and vernacular architecture has brought renewed attention to the yurt as a lightweight, energy-efficient, and environmentally responsive building typology (Tsovoodavaa et al., 2018)[3]. However, despite its cultural prominence and architectural significance, the structural behavior of yurts—particularly under extreme environmental conditions such as high winds or seismic events—remains insufficiently studied from a mechanics and optimization perspective.

To date, scholarly research on yurts has largely centered on their historical, anthropological, and cultural dimensions. Meanwhile, studies focusing on structural mechanics, materials, and

performance optimization remain relatively scarce. In the field of materials science, for example, Xu et al. (2019)[1] conducted field research that highlighted the thermal and humidity regulation challenges inherent to traditional yurt constructions. Their findings suggest that the felt exterior, with its low thermal capacity, inadequately buffers indoor environments from external temperature fluctuations, leading to pronounced diurnal thermal variation. Moreover, its humidity-regulating capacity proved limited under fluctuating atmospheric conditions.

Chen et al. (2022)[2] advanced the modernization of yurt structures by incorporating the traditional wooden framework into cold-formed thin-walled steel configurations. Through systematic low-cycle repeated loading tests, they analyzed the seismic performance of steel yurts, demonstrating that octagonal specimens exhibited nearly 70% higher load-bearing capacity compared to hexagonal designs. Furthermore, the inclusion of an outer protective layer enhanced load-bearing performance by approximately 30%. These findings provide important empirical support for the structural optimization of modern yurts. Similarly, Gheshlaghi and Akbulut (2020)[5] investigated anisogrid lattice structures through algorithmic modeling and FEM simulations, proposing design concepts that may inform the development of lightweight and structurally efficient yurt frameworks.

Despite their unique mechanical properties, traditional yurts—with their timber skeletons and fabric coverings—struggle to meet the heightened structural performance expectations of contemporary architecture. Tsovoodavaa (2019)[4] emphasized the need for systematic structural analysis as a prerequisite for enhancing the resilience and adaptive capacity of yurts in the face of natural hazards. The intersection of energy efficiency and aesthetics has also been explored in related architectural studies. For instance, researchers proposed a modular solar façade system with multilayered design to enhance both visual appeal and solar energy capture—an approach that offers valuable implications for sustainable yurt design.

Additionally, Xu et al. (2013)[6] examined the thermal performance of building envelopes in China's hot summer–cold winter climate zones, emphasizing strategies to enhance indoor thermal comfort and reduce energy consumption. Their findings are relevant to the adaptive redesign of yurts for use in extreme or variable climates. From a cultural standpoint, Segura (2025) [7] offered insight into the spatial composition and sociocultural significance of yurts, thus providing a contextual basis for respectful structural innovation. Furthermore, Ban et al. (2019) [8] examined the high-temperature mechanical properties of stainless-clad bimetallic steel rods, offering data that can inform the selection of materials for climate-resilient yurt structures. Meanwhile, Roovers and De Temmerman (2017) [9] explored deployable scissor-grid mechanisms, presenting novel geometric solutions for portable and modular structural systems akin to yurts.

In summary, while substantial progress has been made in documenting the cultural and historical relevance of yurts, their structural analysis and mechanical optimization—especially under extreme environmental loading—remain underdeveloped areas of inquiry. Addressing this gap, the present study applies finite element analysis (FEA) to investigate the mechanical performance of yurt structures under conditions simulating high wind and seismic loads. By integrating modern structural mechanics with sustainable design principles and cultural sensitivity, this research aims to support both the theoretical advancement and practical modernization of yurt-based architecture for future applications.

2. Methodology

This study employs the Finite Element Method (FEM) to analyze the mechanical performance of a yurt structure under specified extreme loading conditions. The modeling framework involves six key stages: (1) geometric definition of nodes and elements, (2) derivation of element stiffness matrices, (3) coordinate transformation of element matrices, (4) global stiffness matrix assembly, (5)

application of loads and boundary conditions, and (6) solution of the resulting system for displacements and internal forces.

2.1 Geometric Definition of Nodes and Elements

The geometry of the structural model is defined using a nodal coordinate system and element connectivity matrix. Each node is described by its number and three-dimensional coordinates (x, y, z), stored in the NodesInfo matrix. The connectivity of each rod element—represented by a pair of connected node indices—is recorded in the ElesInfo matrix.

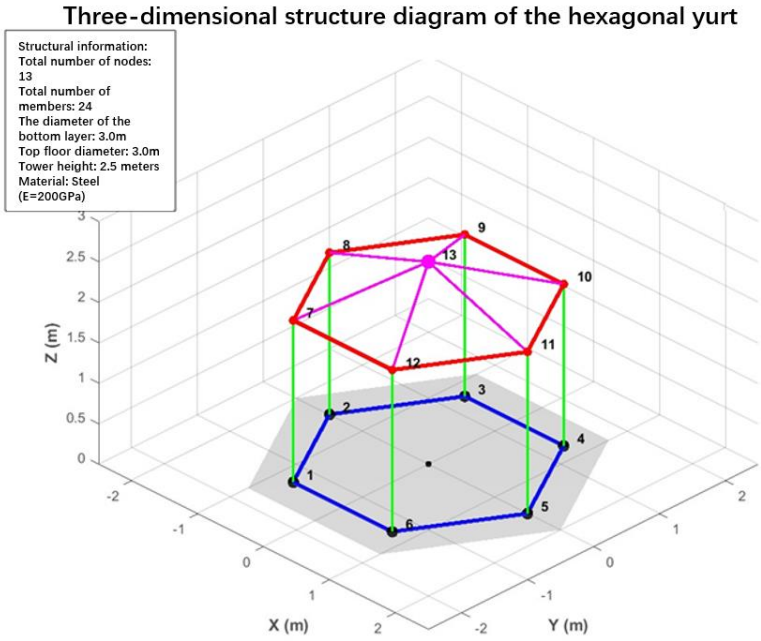

Fig. 1 A simple yurt assembly

In this work, a simple yurt assembly shown in Fig. 1 was modelled, and its node information and element information are given as:

Node Information:

$$\text{NodesInfo} = \begin{bmatrix} 1 & -0.75 & -0.75\sqrt{3} & 0 \\ 2 & -1.5 & 0 & 0 \\ 3 & -0.75 & 0.75\sqrt{3} & 0 \\ \vdots & \vdots & \vdots & \vdots \\ 13 & 0 & 0 & 2.5 \end{bmatrix}$$

Element information:

$$\text{ElesInfo} = \begin{bmatrix} 1 & 1 & 2 \\ 2 & 2 & 3 \\ 3 & 3 & 4 \\ \vdots & \vdots & \vdots \\ 24 & 12 & 13 \end{bmatrix}$$

2.2 Derivation of Element Stiffness Matrix

Each rod element is modeled as a three-dimensional linear elastic member. The element stiffness matrix in the local coordinate system, $\boldsymbol{k_e}$, is given by:

$$\boldsymbol{k_e} = \frac{EA}{L}\begin{bmatrix} 1 & -1 \\ -1 & 1 \end{bmatrix} \tag{1}$$

Where E is the Young's modulus, A is the cross-sectional area, and L is the length of the rod element.

2.3 Coordinate Transformation of Element Stiffness Matrix

Because the bar elements are oriented arbitrarily in space, their local stiffness matrices must be transformed into the global coordinate system. The direction cosines of a given element with respect to the global x, y, and z axes are denoted C_x, C_y, and C_z, respectively. The transformation matrix $\boldsymbol{T}$ is:

$$\boldsymbol{T} = \begin{bmatrix} C_x & C_y & C_z & 0 & 0 & 0 \\ 0 & 0 & 0 & C_x & C_y & C_z \end{bmatrix} \tag{2}$$

The global stiffness matrix for each element, $\boldsymbol{K_e}$, is computed as:

$$\boldsymbol{K_e} = \boldsymbol{T}^T \boldsymbol{k_e} \boldsymbol{T} \tag{3}$$

2.4 Assembly of the Global Stiffness Matrix

The individual element stiffness matrices $\boldsymbol{K_e}$ are assembled into a global stiffness matrix $\boldsymbol{K_{global}}$, sized according to the total degrees of freedom in the system. Each node possesses three degrees of freedom (DOFs: x, y, z), resulting in a global matrix of size $3n \times 3n$, where n is the number of nodes.

Assembly follows these steps:

- Initialize $\boldsymbol{K_{global}}$ as a zero matrix.
- For each element, compute its global stiffness matrix $\boldsymbol{K_e}$.
- Map and superimpose $\boldsymbol{K_e}$ into $\boldsymbol{K_{global}}$ using the DOF indices of the connected nodes n_1 and n_2, filling the following submatrices:

Sub-matrix of K_{global} at ($3n_1$−2:$3n_1$, $3n_1$−2:$3n_1$).
Sub-matrix of K_{global} at ($3n_1$−2:$3n_1$, $3n_2$−2:$3n_2$).
Sub-matrix of K_{global} at ($3n_2$−2:$3n_2$, $3n_1$−2:$3n_1$).
Sub-matrix of K_{global} at ($3n_2$−2:$3n_2$, $3n_2$−2:$3n_2$).

2.5 Loads and Boundary Conditions

Gravity Load

The structure's total weight, assumed to be W=180 N, is evenly distributed as vertical concentrated loads among the six bottom support nodes. The corresponding entries in the global load vector $\boldsymbol{F}$ are:

$$F(3{:}\,3{:}\,18) = -\frac{W}{n} \tag{4}$$

Wind Load

Wind loading is calculated using the drag-force equation:

$$F_{wind} = \frac{1}{2} C_d \rho V^2 A \tag{5}$$

Where C_d is the drag coefficient, ρ is the air density, V is the wind speed, and A is the projected area. The resulting wind force, $F_{wind} = 1984.5\ N$, is evenly distributed as horizontal concentrated

loads in the x -direction at the same six bottom nodes:

$$F(1:3:18) = \frac{F_{wind}}{n} \tag{6}$$

2.6 Solution for Displacements and Forces

Letting $\boldsymbol{u}$ represent the global displacement vector, the system of equations is:

$$\boldsymbol{K_{global}u = F} \tag{7}$$

With m degrees of freedom fixed (e.g., fully constrained support nodes), the displacement of the remaining free DOFs is calculated by solving:

$$\boldsymbol{u}_{unknown} = \boldsymbol{K_{global}^{-1}}(m+1:end, m+1:end)\boldsymbol{F}(m+1:end) \tag{8}$$

The complete displacement vector is then reconstructed as:

$$\boldsymbol{u} = \begin{bmatrix} 0 \\ 0 \\ 0 \\ \vdots \\ u_{unknown} \end{bmatrix}$$

Once nodal displacements are known, internal forces and element stresses are computed based on deformation in each bar element using classical structural mechanics formulas.

3. Results and Discussion

3.1 Load Case Analysis

The total weight of the structure is 180 N. To simulate actual support conditions, this gravity load was evenly distributed among six bottom support nodes, with each node bearing a vertical force of -30 N (z-direction). The wind load, calculated using standard aerodynamic principles—including the drag coefficient (Cd), air density (ρ), wind speed (V), and projected area (A)—resulted in a total horizontal force of 1984.5 N. For simplification, this force was equally applied to the x-direction of the same six bottom nodes, assigning each approximately 330.75 N.

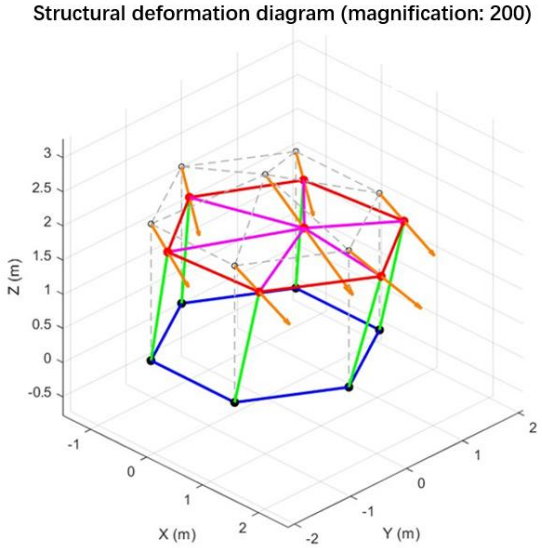

Fig. 2 Deformation of yurt assembly

Analysis of internal forces indicated that vertical support elements experienced the highest compressive forces, up to 268.3 N, while bottom hexagonal members primarily resisted tensile forces, with a maximum of 142.1 N. These tensile elements played a crucial role in base stabilization under wind loading. Forces in the upper elements and diagonal braces were minor, suggesting effective load transfer through primary members.

Stress analysis showed maximum compressive and tensile stresses of 0.89 MPa and 0.47 MPa, respectively. Compared to the steel yield strength of 235 MPa, this corresponds to safety factors of 264 (compression) and 500 (tension), far exceeding conventional design safety thresholds.

3.2 Displacement Analysis

Under the applied gravity and wind loads, the displacement results clearly demonstrated the structure's deformation characteristics, as shown in Fig. 2. The bottom nodes (1-6) were fully fixed, thus exhibiting zero displacement. The middle-layer nodes (7-12) showed slight deformation, with a maximum horizontal displacement of 2.3mm and a maximum vertical settlement of 1.4mm. The top node (13) experienced the largest deformation within the entire structure, with a horizontal displacement of 3.5mm and a vertical settlement of 2.5mm.

Overall, the structure's deformation pattern was an inclination towards the wind direction (+x-axis), accompanied by a slight overall settlement. Notably, even the maximum displacement of 3.5mm is well below the generally acceptable deformation limits in engineering design (e.g., L/300). This strongly indicates that the current yurt structure design possesses sufficient rigidity, capable of effectively resisting external loads and ensuring its stability and safety during use.

3.3 Support Reaction Results

The analysis of support reactions at the bottom nodes is crucial for evaluating the structure's overall force equilibrium and load transfer efficiency.

Upon summing the support reactions: the total reaction force in the x-direction approximately equals the total wind load experienced by the structure (1984.5N); the total reaction force in the y-direction is zero; and the total reaction force in the z-direction is approximately equal to the total gravity load on the structure (180N). These balanced verification results collectively confirm that the yurt structure is in a stable equilibrium state under the applied load conditions.

3.4 Internal Force and Stress Analysis

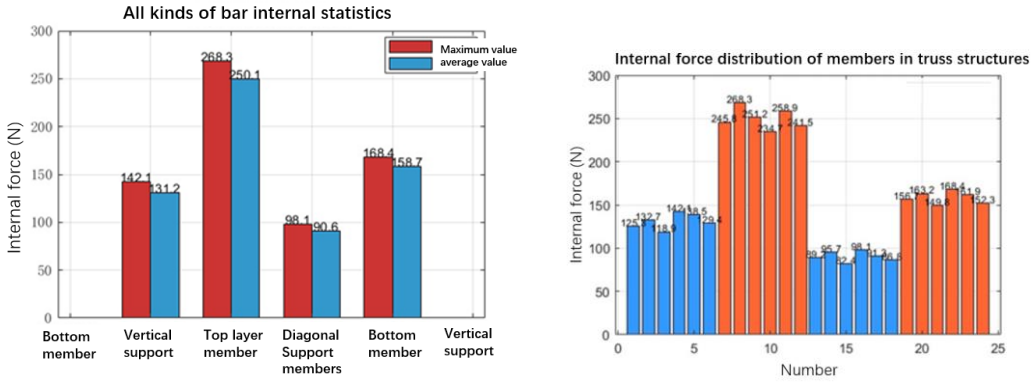

Fig. 3 Internal forces in rod members of yurt assembly

As shown in Figs. 3 and 4, an analysis of the internal forces in the rod elements revealed that

vertical supporting elements bore the maximum compressive force (268.3N), while bottom horizontal elements primarily experienced tensile forces (up to 142.1N), indicating an efficient and clear load transfer path. More critically, stress calculations showed that the maximum compressive stress was only 0.89MPa, and the maximum tensile stress was 0.47MPa. Assuming all elements use material with a cross-sectional area of A=3×10−4m2, when comparing these stress values to the steel's yield strength (235MPa), the resulting safety factors were remarkably high: 264 for compression and 500 for tension. These safety factors far exceed the typical engineering design requirements of 2-3, clearly indicating that the current yurt structure design is highly conservative.

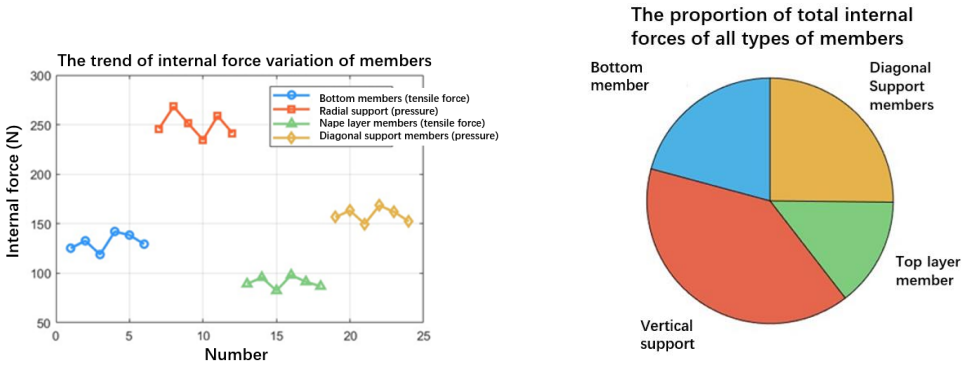

Fig. 4 Difference of internal forces in different rod members

4. Conclusion

This study utilized the Finite Element Method (FEM) to analyze the mechanical performance of a yurt structure under combined gravity and wind loads, offering valuable insights for its performance assessment and optimization. The research not only confirms the inherent strength and safety of the yurt structure when subjected to extreme loads but also highlights the potential for optimizing its design to enhance material efficiency and economic benefits. These findings provide crucial theoretical basis and technical guidance for the modernization of yurt structures, improving their disaster resilience, and expanding their application in sustainable architecture.

References

[1] Xu, Guoqiang, Hong Jin, and Jian Kang. "Experimental study on the indoor thermo-hygrometric conditions of the Mongolian yurt." Sustainability 11.3 (2019): 687.
[2] Chen, Ming, et al. "Experimental investigation of cold-formed thin-walled yurts with bolted connections under low-cyclic reciprocating loading." Thin-Walled Structures 172 (2022): 108903.
[3] Tsovoodavaa, Gantumur, et al. "A review and systemization of the traditional Mongolian yurt (GER)." Pollack Periodica 13.3 (2018): 19-30.
[4] Tsovoodavaa, Gantumur. "A Transportable and Energy Optimized Residential Building Architectural Design for the Mongolian Climate." (2019).
[5] Gheshlaghi, Reza Mohammadzadeh, and Hamit Akbulut. "Modeling and Analysis of Anisogrid Lattice Structures Using an Integrated Algorithmic Modelling Framework." Computational Research Progress in Applied Science & Engineering 6 (2020).
[6] Xu, Luyi, et al. "Building energy saving potential in Hot Summer and Cold Winter (HSCW) Zone, China—Influence of building energy efficiency standards and implications." Energy Policy 57 (2013): 253-262.
[7] Segura, Jesse. "Reimaging housing: a perspective from the Mongolian yurt." Housing Studies (2025): 1-25.
[8] Ban, Huiyong, et al. "Mechanical properties of stainless-clad bimetallic steel at elevated temperatures." Journal of Constructional Steel Research 162 (2019): 105704.
[9] Roovers, Kelvin, and Niels De Temmerman. "Geometric design of deployable scissor grids consisting of generalized polar units." Journal of the International Association for shell and spatial structures 58.3 (2017): 227-238.